CHAPTER 3

METHODOLOGY

3.1 Introduction

This section describes all the modelling procedures to achieve the planned objectives. The primary goal of this study is to develop a conceptual model for optical properties and ruby stone valuation using a CCD tomography method. The research defined three objectives in this study. The flow of the objective is shown in Figure 3.1 flow chart below. Objective 1 was to investigate the light intensity of the ruby stones based on their theoretical values, such as light refraction and absorption effect. The first procedure is to examine the light intensity of ruby stone based on theoretical value via the CCD tomography approach and GIA database (Fuller et al., 2014). In this phase, light attenuation due to absorption and refraction was considered to investigate their relationship with the refractive index of the ruby stone established from the ruby stone. The consideration of those light attenuation effects is due to the different types of medium passes by the light source with different refractive index and attenuation coefficient values (Idroas, 2004).

Objective 2 involved designing a conceptual model of the CCD tomography technique using the LabVIEW software. For this purpose, an octagon orientation concept for CCD and the placement of the ruby stones for conceptual modeling were developed. The octagonal orientation gives a wide coverage area of the ruby stone measured.

The mathematical expression derived from Objective 1 was used for the simulation of conceptual modeling of CCD tomography technique and ruby stone. The result of the simulation is the three-dimensional image. The analysis of the pixel value is done to evaluate the capability of CCD tomography and LabVIEW software to validate that this system can be used to quantitatively grade ruby stone. As such, the three-dimensional image from the simulations and experiments were compared and analyzed through statistical and relative error analysis. Figure 3.2 provides a flow chart of the methodology of this study.

3.2 CCD Tomography System Modeling

This present study used a CCD tomography system to validate the optical properties of ruby stones. This method was selected based on the findings of extant studies, which concluded that a CCD and tomography system could be used to differentiate between different levels of object transparency successfully (Jamaludin, Abdul Rahim, et al., 2016, 2018; Jamaludin, Rahim, et al., 2018; Jamaludin, Rahim, Rahim, et al., 2017). The block diagram of this present study consists of three important parts; the object of interest (ruby stone) and hardware part, interface, and software (Figure 3.1).

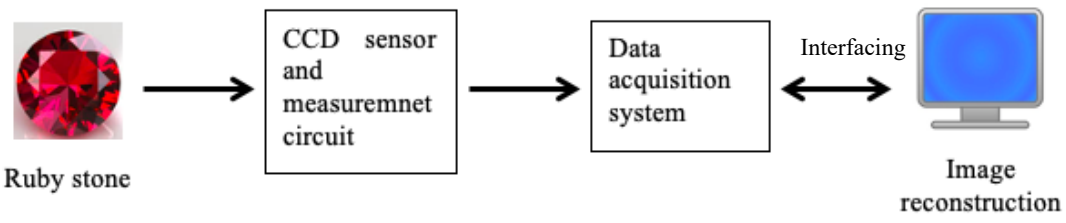

Figure 3.1: Block Diagram of The CCD Tomography System

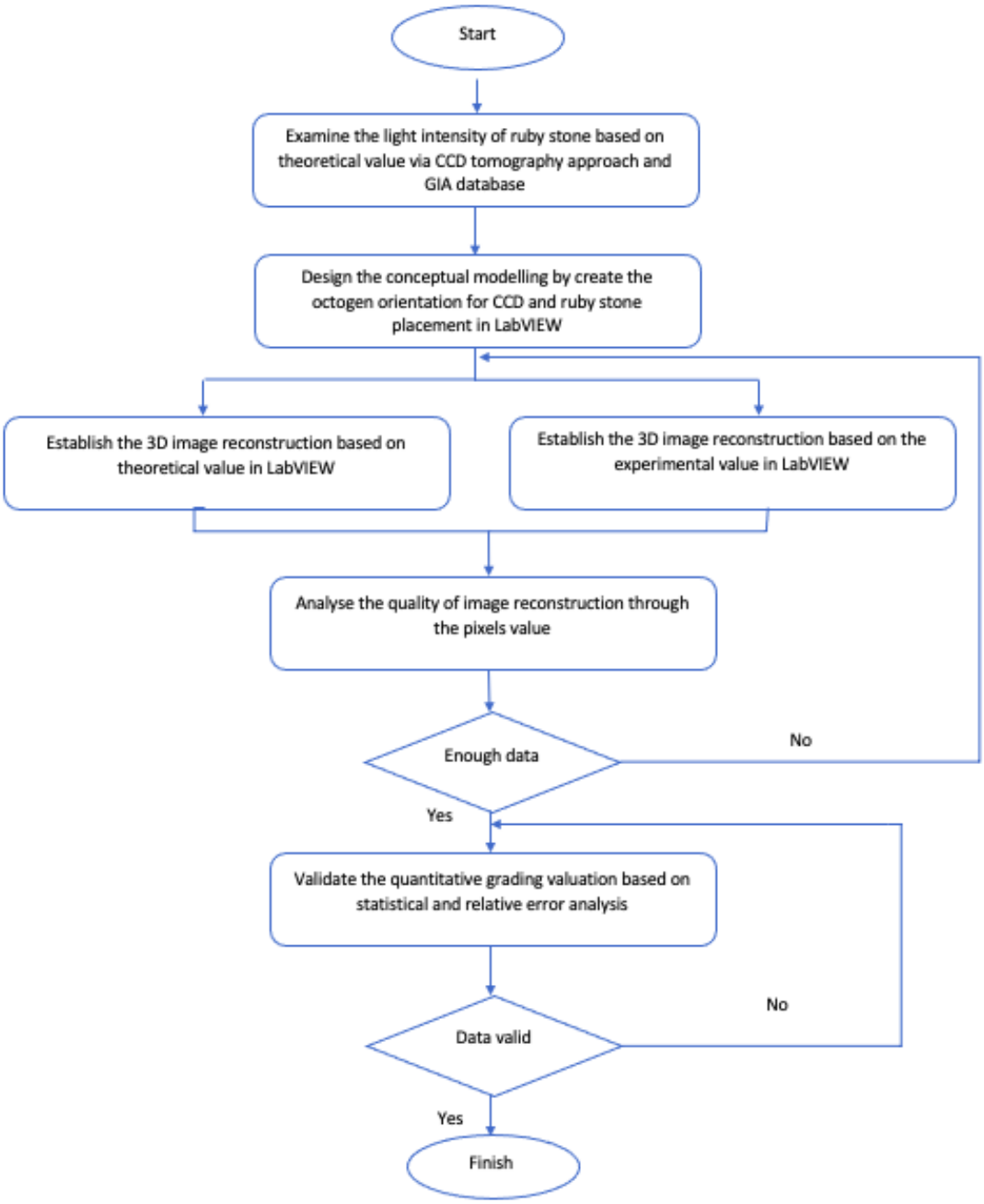

Figure 3.2: Flow Chart of The Methodology of This Study

The hardware used in this present study included CCD sensors, electronic measurement circuits, and the measured object, i.e., ruby stones. Ruby stones measuring 19.18 mm in diameter were used to investigate optical properties. This size of the ruby

stone is chosen because it is compatible and convenient for the SONY™ ILX551A CCD Linear Sensor to measure and analyze (Jamaludin, 2016). Figure 3.3 depicts the diameter of a sample ruby stone; ruby stone *z*; as measured using a vernier calliper.

Figure 3.3: Diameter of Ruby Stone *Z* As Calculated Using a Vernier Calliper

The data acquisition system (DAS) was used to interface the hardware; i.e., the CCD sensor and measurement circuit; to the image reconstruction software. The choice of tomography depends on the medium of interest as it affects the choice of sensor used to measure the medium of interest (Wahab et al., 2014). As such, this present study used a CCD sensor for the tomography process to produce the quantitative grades of ruby stones by analyzing their clarity.

3.2.1 Theoretical Value for CCD Voltage Output

In order to obtain a theoretical CCD voltage output, a study was conducted using a laser diode (0.3 lux value) in a SONY™ ILX551A CCD Linear Sensor (Jamaludin, 2016; Mohd Rahalim et al., 2022). As a laser diode provides a monochromatic light source, it is the best choice of the transmitter. The experimental setup for the 'On' and 'Off' conditions is shown in Figure 3.4.

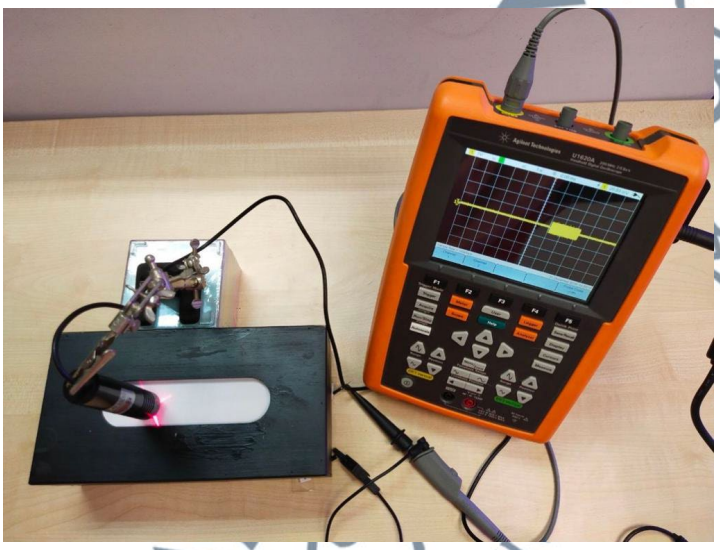

Figure 3.4: Experimental Set Up for laser 'On' and 'Off'

Table 3.1 presents all experimental values derived from the CCD Tomography System using the CCD output voltage values when the laser was kept 'On' and 'Off' in addition to their respective light intensity values.

Table 3.1: CCD Voltage Outputs and Laser Light Intensities in Off and On Mode

Condition of Laser	CCD Voltage Output (V)	Light Intensity
Off	4.2817	0
On	1.5834	1

This experiment passes the light beam through the air before it hits the CCD sensor. Figure 3.5 indicates that the laser intensity was inversely proportional to the CCD voltage output based on the experimental results. The equation depicts the correlation between light intensity and CCD voltage output.

$$V = -2.78I + 4.3 \quad (3.1)$$

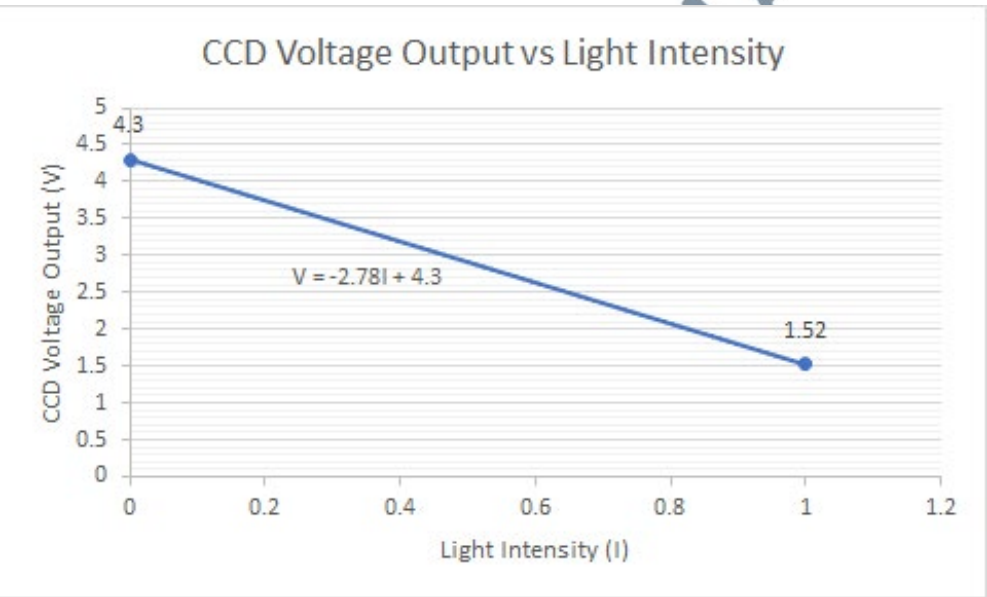

Figure 3.5: CCD Voltage Output as A Function of Light Intensity

As seen in Figure 3.5, the voltage value obtained from the equation was V = −2.78I + 4.3. The voltage value based on the final light intensity ratio was further investigated and is explained in the Results section.

3.3 Gemmology Tools Software

This present study investigated the refractive index of ruby stones to analyze its optical property further. Figure 3.6 shows the range of the refractive index of ruby stone as stated in the databases of the Gemology Tools software.

Gemstone	Species	Group	Refractive Index
Ruby	Corundum		1.770-1.762 +.009 -.005

Source: Fuller et al. (2014)

Figure 3.6: Refractive Index Range of Rubies from The Gemmology Software Tools Databases

The ruby stone shows the highest refractive index (RI) value of 1.770, while the lowest RI value was 1.762. These two values were then compared in terms of their image reconstruction based on the final light intensity ratio of the optical properties of the rubies. The following mathematical expression was used by using the RI obtained from the Gemology Software Tools' databases (Fuller et al., 2014).

3.4 Mathematical Expression for the CCD

In this study, Objective 1 was developed to investigate the light intensity of the ruby stones based on their theoretical values, such as light refraction and absorption effect. The mechanism was obtained by experimenting with the CCD and tomography system. The two types of experiments conducted in this present study are:

1. The system includes a ruby stone, laser, and CCD apparatus (System A).
2. The system includes a ruby stone and CCD (System B).

As shown in Figure 3.7 below, the light passed through 2 differing mediums, the air and ruby stone, while the laser acted as the light source. However, in Figure 3.8, the light reflection reached the CCD directly without the laser as the light source.

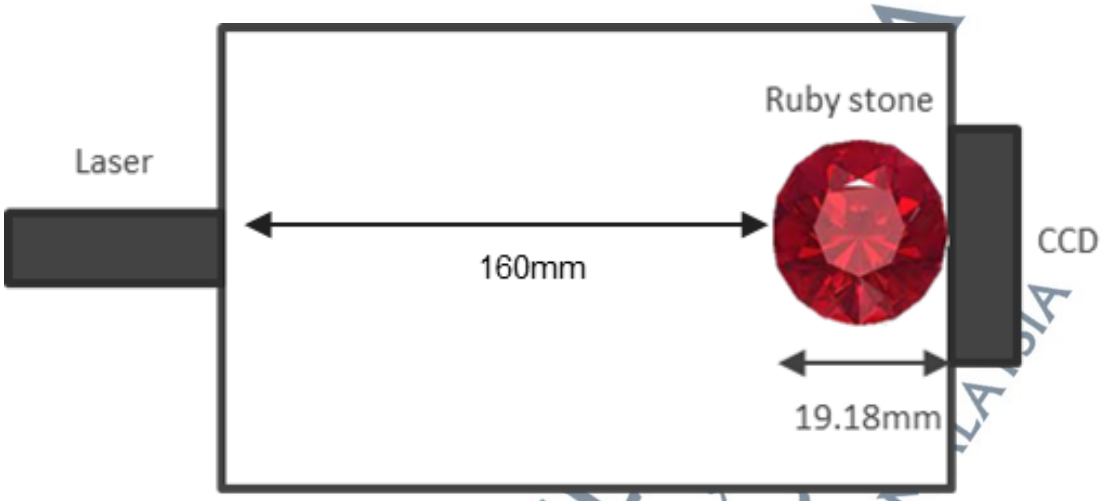

Figure 3.7: Flow of Light Through the Ruby Stone and The CCD As Seen in System A

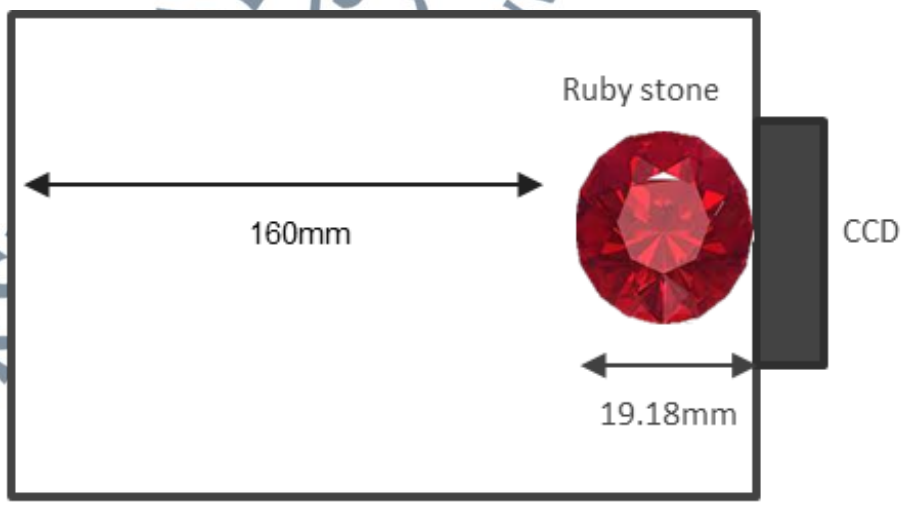

Figure 3.8: Flow of Light Through the Ruby Stone and The CCD As Seen in System B

Earlier studies have stated that light attenuation occurs when light travels through a transparent or translucent object due to different phenomena like light reflection, absorption, and scattering (Jamaludin, 2016). Based on Nassau (2003), the light scattering could be ignored because the wavelength of the incident light that was used (laser light) was smaller than the diameter of the object of interest. This statement is also supported by Idroas (2004), where the light diffraction and light scattering effect could be ignored if the diameter of the object under study is greater than the laser diode wavelength. In this research, the size of ruby z used for analysis is 19.18 mm. Meanwhile, the laser diode which acts as the transmitter in this modeling study is the red laser with 650 nm wavelength. Therefore, the light attenuation due to light scattering and light diffraction is imperceptible in this research. Hence, the research used two different types of algorithms for the simulation, wherein light attenuation was due to:

- Light absorption
- Light reflectance

According to existing studies, these two types of light phenomena were considered as a CCD can distinguish between the different levels of object transparency in a tomography system (Jamaludin & Abdul Rahim, 2016).

3.4.1 Light Absorption

Light gets attenuated when it passes from medium 1 to medium 2 which has two different density level (Nassau, 2003), wherein attenuation occurs because of absorption (Idroas 2004). The different mediums possess their respective coefficient values, α, which are used in the Beer-Lambert Law as described below (Idroas, 2004; Jamaludin, 2016):

$$I_{out} = I_{in} e^{-\alpha x} \quad (3.2)$$

Based on the above formula, the output light intensity Iout of this research is gained by multiplying the light intensity input (I_{in}) by the exponential attenuation of the medium density after the light passed through the medium. α refers to a linear attenuation coefficient of substance, while x indicates the thickness or distance of the medium penetrated by the light beam. Table 3.2 presents the linear attenuation coefficient values (Jamaludin, Abdul Rahim, et al., 2016) along with the RI values (Fuller et al., 2014) for the two different mediums investigated in this study. The linear attenuation coefficient of the ruby stone was presumed to be similar to Perspex (Idroas, 2004).

Table 3.2: Linear Attenuation Coefficient and Refractive Index of Air and Ruby Stones

Medium	Linear attenuation coefficient (mm^{-1})	Refractive index
Air	0.00142	1.0003
Ruby stone	0.00310	1.762-1.770

Source: Jamaludin (2016)

3.4.2 Light Reflectance

The photo (light) energy decreased when the light beam passed through different mediums or passed through an object near the medium. Light reflectance can be expressed as follows (Idroas, 2004; Jamaludin, 2016):

$$I_{Final\ reflection1} = I_{initial} - \left[I_{initial} \left(\frac{n_2 - n_1}{n_2 + n_1} \right)^2 \right] \quad (3.3)$$

$$R = \left(\frac{n_2 - n_1}{n_2 + n_1} \right)^2 \quad (3.4)$$

R = *Reflection ratio*

n_1 = *Transmitted refractive index*

n_2 = *Incidence refractive index*

The light attenuations for the two mediums, owing to light reflectance and absorption, can be integrated for developing a mathematical expression in this study. Section 3.4.3 provides the full mathematical expression when a 19.18 mm-diameter ruby stone is situated between the measurement area and a laser beam directed to the CCD sensor (System A). In contrast, Section 3.4.4 is the mathematical expression for System B.

3.4.3 Mathematical Expression for System A

The first situation in the CCD linear sensor system occurs when light travels from the laser toward the ruby. As this light hits the ruby's surface, reflection occurs where the light gets reflected away from the ruby. In this situation, the light intensity calculation involves the light reflectance equation, which is equation (3.3). The incidence RI in this situation will be the RI of air, which is equal to 1 (Idroas, 2004). The transmitted RI will be the RI of the ruby, with a value of 1.762. Hence, the light intensity during the first situation will be calculated using equation (3.3) as follows:

$$I_1' = I_i - I_{reflection1} = I_i - \left[I_i \left(\frac{n_{rubystone} - n_{air}}{n_{rubystone} + n_{air}} \right)^2 \right] \quad (3.5)$$

$$I_1' = I_i - \left[I_i \left(\frac{1.762 - 1}{1.762 + 1} \right)^2 \right] = 0.9238 I_i \quad (3.6)$$

When the light enters the ruby, it gets absorbed. Thus, the light absorption equation (3.2) will calculate the light intensity in this second situation. The α of the ruby is $0.003\ \mathrm{mm}^{-1}$, and x of the ruby is 19.18 mm. Hence, the light intensity of the ruby is determined by the following equation.

$$I_2 = I_1' e^{-(0.003mm^{-1}x19.18mm)} = 0.99I_1 \tag{3.7}$$

$$I_2 = 0.9239I_i \tag{3.8}$$

In the third situation, the light travels out of the ruby toward the CCD linear sensor. This situation involves the reflection of light from the surface of the ruby toward the CCD linear sensor. Thus, equation (3.3) will be used in this situation, where the transmitted RI is the RI of the air and the incidence RI is the RI of the ruby. The calculation is performed using the following equations:

$$I_2' = I_2 - I_{reflection2} = I_2 - \left[I_2\left(\frac{n_{air}-n_{rubystone}}{n_{air}+n_{rubystone}}\right)^2\right] \tag{3.9}$$

$$I_2' = I_2 - \left[I_2\left(\frac{1-1.762}{1+1.762}\right)^2\right] = 0.9238I_2 \tag{3.10}$$

$$I_2{}' = 0.8478I_i \tag{3.11}$$

According to Equation 3.11, the theoretical final light intensity ratio, for system A, with a minimum RI of $n_{rubystone}$ of 1.762 and a ruby stone of $0.003\ \mathrm{mm}^{-1}$ is $\frac{I_2'}{I_i}$ = 0.8478. The mathematical expression was repeated with a maximum RI of 1.770. The table of results is shown in Chapter 4.

3.4.4 Mathematical Expression for System B

The mathematical expression was repeated with a different image reconstruction system, System B, which did not have a laser for a transmitter. The light reflection from the ruby stone passed directly through to the CCD and ignored the light absorption phenomena in this mathematical expression, as there is no specific size diameter for a medium transverse within the light (air). The mathematical expression for System B is as follows. The Ii (light intensity) is decreased because of reflection at the Air-ruby stone interface. The light intensity calculation involves the light reflectance equation, which is equation (3.3). The incidence RI in this situation will be the RI of air, which is equal to 1. The transmitted RI will be the RI of the ruby, with a value of 1.762.

Hence, the light intensity during the first situation will be calculated using equation (3.3) as follows:

$$I_1' = I_i - I_{reflection1} = I_i - \left[I_i \left(\frac{n_{rubystone} - n_{air}}{n_{rubystone} + n_{air}} \right)^2 \right] \quad (3.12)$$

$$I_1' = I_i - \left[I_i \left(\frac{1.762 - 1}{1.762 + 1} \right)^2 \right] = 0.9238 I_i \quad (3.13)$$

According to Equation 3.13, the final light intensity ratio for light passing through the ruby stone with an $n_{rubystone}$ of 1.762 and a rubystone of $0.003\ mm^{-1}$is $\frac{I_2'}{I_i}$ = 0.9238. The mathematical expression was repeated with a maximum RI of 1.770. The table of results is shown in Chapter 4.

3.5 Software Development

Generally, a simulation model can be used for handling real-world problems in an orderly and safe manner. It offers a convenient technique for analysis that helps in discussing, verifying, and comprehending the problems. A simulation model offers valuable solutions across all disciplines and sectors as it presents a clear insight into complex systems. The simulation was an important aspect of this present study as it validates the ability of the CCD tomography system to establish a grading valuation of ruby stones based on clarity.

3.5.1 LabVIEW

LabVIEW (Laboratory Virtual Instrument Engineering Workbench, National Instruments) is a reliable system engineering software that offers a development environment for a visual programming language (Aspey et al., 2008). Owing to the different operating systems available, such as Microsoft Windows, Linux, many versions of Unix, and macOS, LabVIEW software can be used for instrument control, data acquisition, and industrial automation. LabVIEW consists of two types of windows: the block diagram, which uses graphical representations of functions to complete calculations and control the front panel objects, and the front panel, which perform as the user interface (NI Learning Center - NI, n.d.). This section will discuss the application of LabVIEW programming software to produce the modeling for the grading valuation of ruby stone.

3.5.1.1 Mathematical Expression of Rubies and CCD Tomography in LabVIEW

The previous step was to be used in modeling the LabVIEW program based on the interaction of light in the pipeline of an optical tomography system. Figure 3.9 and Figure 3.10 present the block diagram of the graphical code for the light attenuation owing to light absorption and light refraction, respectively, derived from the mathematical equations presented above.

i. Light absorption equation and the block diagram of graphical code for the LabVIEW model

$$\mathrm{I_{out}} = \mathrm{I_{in}} e^{-\alpha x} \tag{3.14}$$

$$I_4 = 0.6408 I_i \tag{3.15}$$

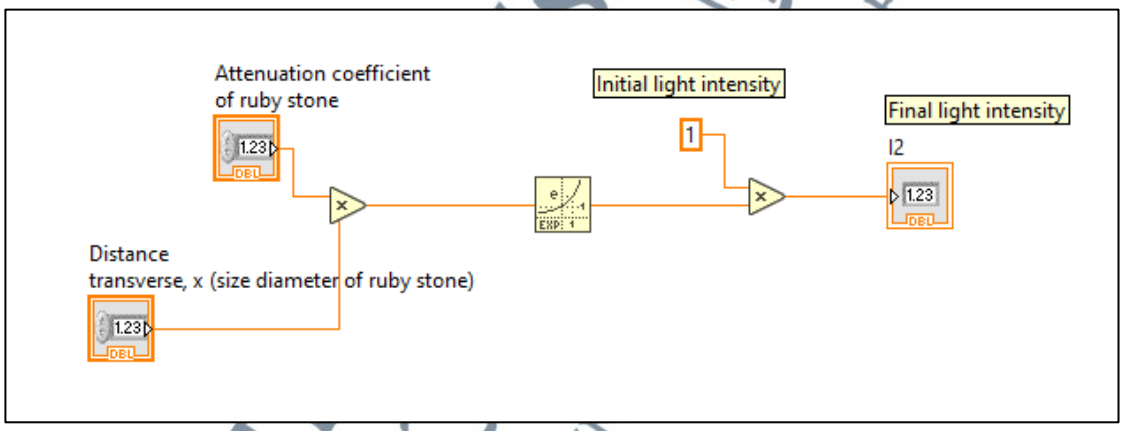

Source: LabVIEW Programming Software Tools

Figure 3.9: The LabVIEW Graphical Code for Calculating Light Absorption

Figure 3.9 shows two types of controllers, the attenuation coefficient of ruby stone, 0.003 $\mathrm{mm^{-1}}$ (Idroas, 2004), and the *x* value, which is the distance transverse representing the size diameter of the ruby stone (19.18 mm). Meanwhile, the constant is always 1 (Jamaludin, 2016), which is the $\mathrm{I_{in}}$ (initial light intensity). Based on equation

(3.14), the initial light intensity value is multiplied by the exponential power of multiplication for the attenuation coefficient of ruby stone and the size diameter of ruby stone to get the final light intensity value (I_{out}). The I_{out} is the indicator represented in this LabVIEW block diagram of graphical code for calculating light absorption.

ii. Light reflection equation and a graphical code for the LabVIEW model.

$$I_{Final\ reflection1} = I_{initial} - \left[I_{initial}\left(\frac{n_2-n_1}{n_2+n_1}\right)^2\right] \quad (3.16)$$

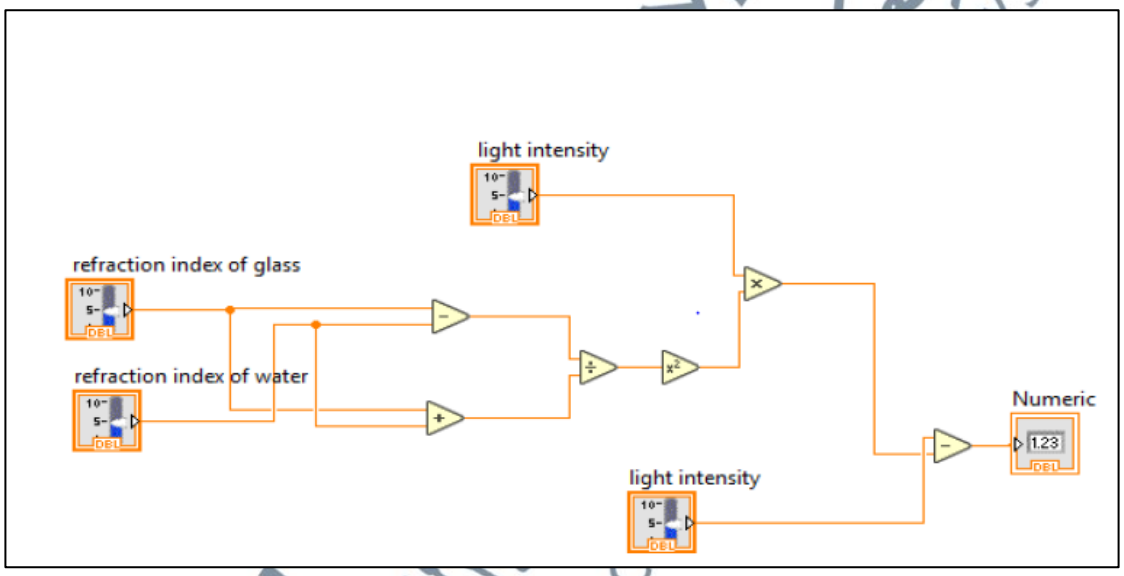

Source: LabVIEW Programming Software Tools

Figure 3.10: LabVIEW Coding to Calculate Light Reflection

Figure 3.10 shows five types of nodes referring to the equation (3.16). The node used is the subtraction, division, multiplication of two, and common multiplication. There are two constants: the RI of air and ruby stone, n_2 and n_2. The numeric from the block diagram is the indicator that represents the IFinal reflection1. Meanwhile, the

light intensity depends on the previous calculation of this mathematical equation. A further explanation has been explained in the next section.

iii. Final light intensity equation that was obtained from the previous calculation and the graphical code for the LabVIEW model with a front panel view for System A as shown in Figure 3.11 and Figure 3.12 respectively. The light equation for this LabVIEW block diagram of graphical coding is as in (3.7), (3.8), and (3.9).

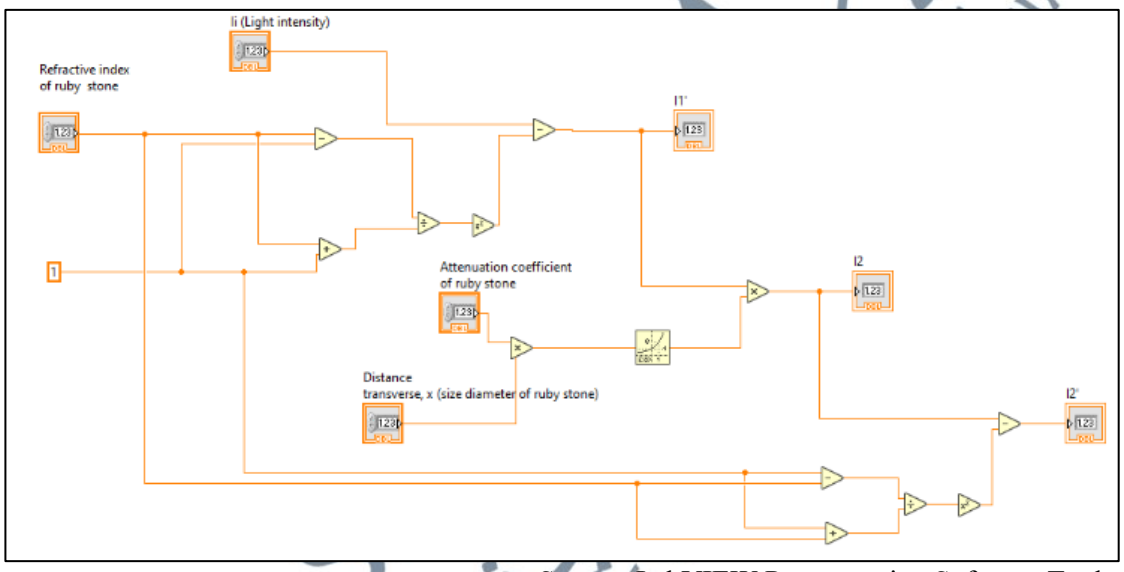

Source: LabVIEW Programming Software Tools

Figure 3.11: Graphical Code for The LabVIEW Model for System A

Figure 3.11 is the combination and sequence from equations (3.7), (3.8), and (3.9). The light intensity value, I_1' will be the indicator for equation (3.7) and the controller for equation (3.8). Next, the light intensity value, I_2 will be the indicator for equation (3.8) and the controller for equation (3.9). Finally, the light intensity value, I_2' will be the equation (3.9) indicator. From the graphical code in the LabVIEW block

diagram of Figure 3.9 to Figure 3.11, two important values will be considered: the attenuation coefficient (Idroas, 2004) and the RI of the ruby stone (Fuller et al., 2014), as shown in the front panel of Figure 3.12.

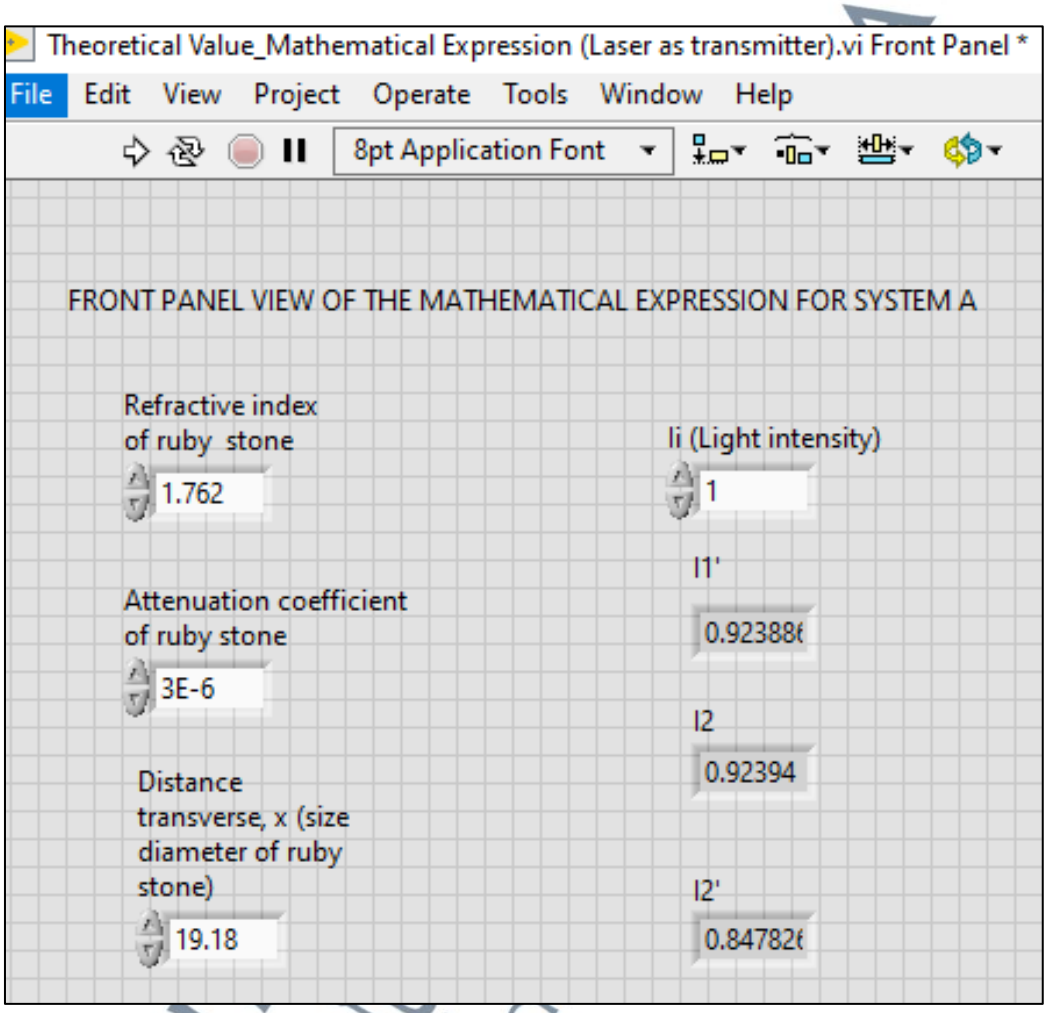

Source: LabVIEW Programming Software Tools

Figure 3.12: Front Panel View of LabVIEW for System A

For System A, the light attenuation due to the reflection and absorption is considered as the laser acts as the source of light in this CCD tomography system approach. The front panel in Figure 3.12 gives better visualization of the user interface as code in the

LabVIEW block diagram in Figure 3.11. As the RI, attenuation coefficient, and size diameter of ruby stone z is 1.762, 0.003 mm^{-1}, and 19.18 mm, respectively, the final light intensity value I_2' for system A is 0.8478. The result of this calculation will be explained in Chapter 4.

iv. Final light intensity equation that was obtained from the previous calculation and the graphical code for the LabVIEW model with a front panel view for System B as shown in Figure 3.13 and Figure 3.14 respectively.

$$I_1' = I_i - I_{reflection1} = I_i - \left[I_i \left(\frac{n_{rubystone} - n_{air}}{n_{rubystone} + n_{air}}\right)^2\right] \quad (3.17)$$

$$I_1' = I_i - \left[I_i \left(\frac{1.762-1}{1.762+1}\right)^2\right] = 0.9238 I_i \quad (3.18)$$

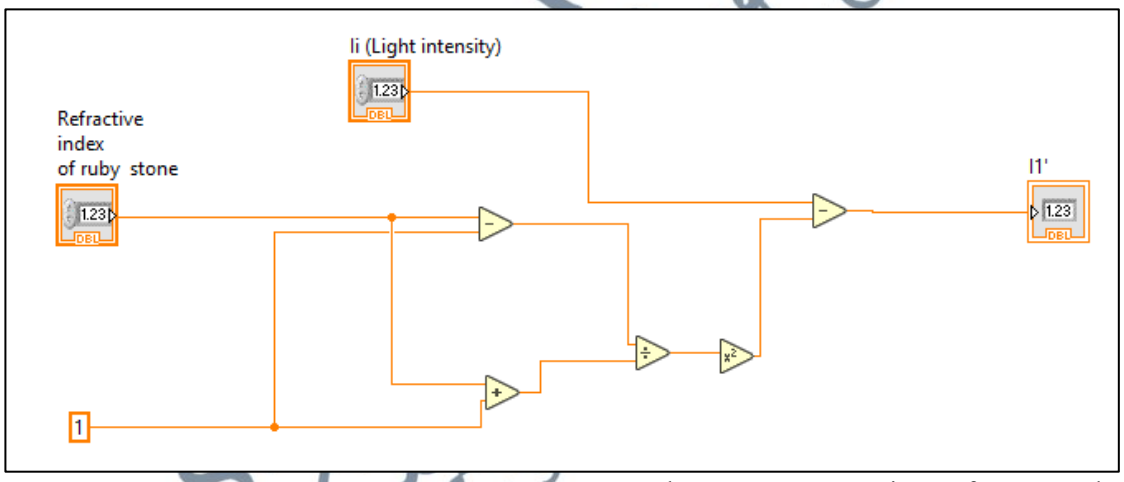

Source: LabVIEW Programming Software Tools

Figure 3.13: Graphical Code for The LabVIEW Model for System B

For System B, the light attenuation effect is only the light reflection since there is no light source from the laser propagating through the ruby stone; hence, no light absorption occurs. The light reflection block diagram in the LabVIEW software is

shown in Figure 3.13 as in Equation 3.18. The front panel in Figure 3.14 below shows that for RI value of the ruby stone is 1.762 and, the initial light intensity I_i is 1, the final light intensity value, I_1' received by the CCD is 0.9238.

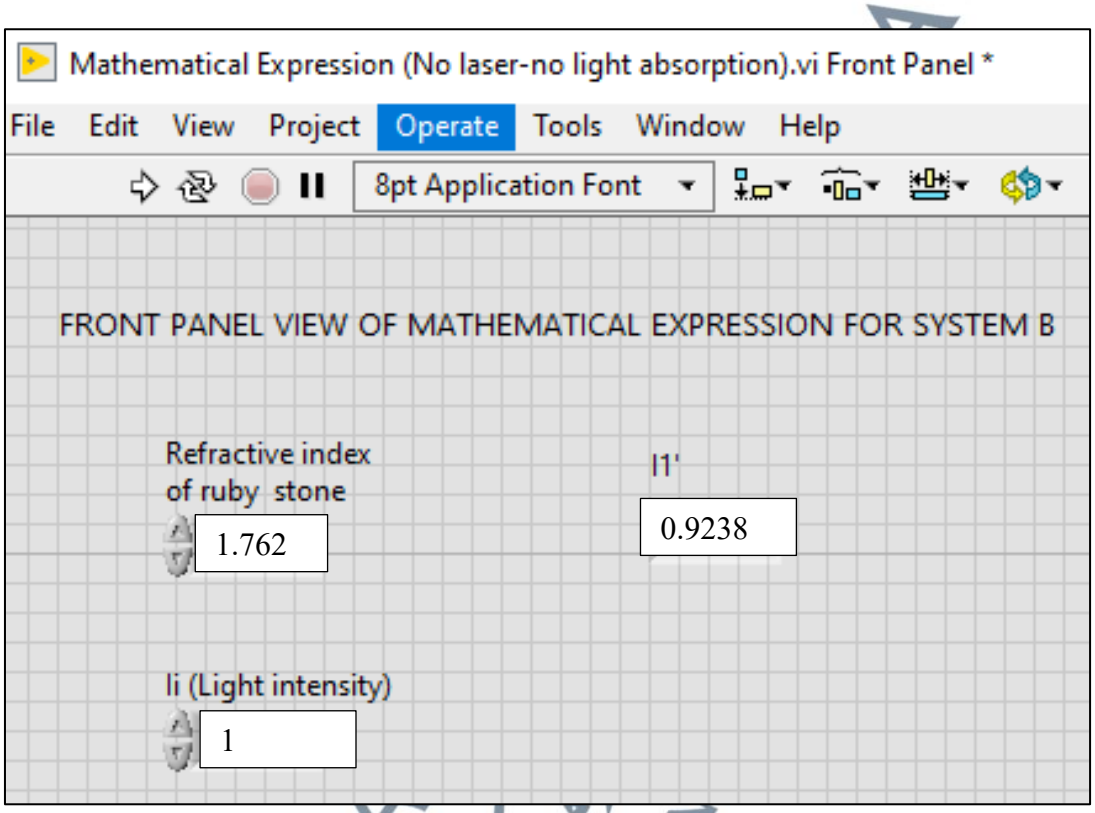

Source: LabVIEW Programming Software Tools

Figure 3.14: Front Panel View of LabVIEW for System B

3.5.2 Image Reconstruction System Modeling

3.5.2.1 Transmitter and Sensor Orientation

Combining the rectilinear and orthogonal projection in one plane generates an octagonal shape for the sensor orientation. Multiple projections help decrease the smearing effect during image reconstruction (Maurice, 2012). The Sony ILX551A has 2048 pixels (size range of 14 µm ×14 µm). The total length of the sensitive pixels is

28.6720 mm. Figure 3.15 depicts the sensor orientation of these CCDs. They were arranged in an octagon and parallel to the incident light (laser) to provide wide coverage of the ruby stone diameter. The image captured is displayed in 64 x 64 image resolution but in different numbers of views. A view is a term for the single combination of emitter and detector aligned in a parallel array known as projection (Ferns Icon, n.d.). Each of the sequences of laser and CCD will provide a single projection, as shown in the figure below.

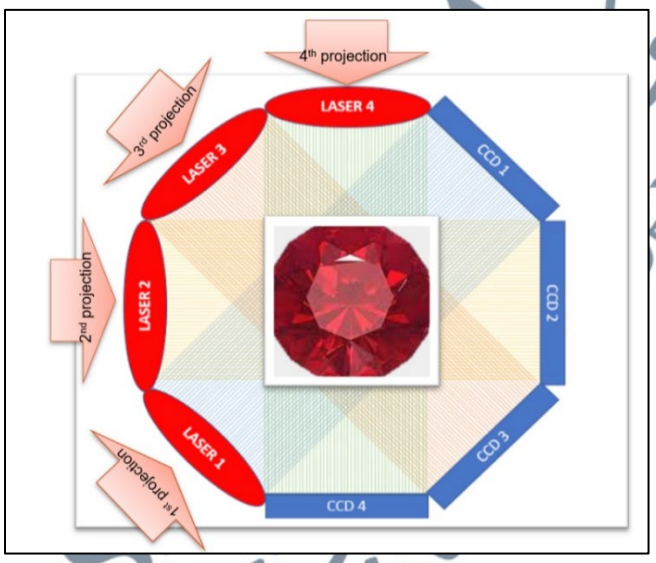

Figure 3.15: CCD And Laser Light Source

3.5.2.2 Sensor Views

The captured image can be displayed in the 64 × 64 image resolution, however, using numerous views. As shown in Figure 3.15, every CCD presents 40 views of the LBP image. A view refers to a single combination of the emitter and detector aligned in the parallel array called projection (Jamaludin, 2016). Every view presents the no. of

sensors and pixels in the CCD. Figure 3.16 below shows the SONY™ ILX551A CCD Linear Sensor used in this research, such as the experimental setup in Figure 3.16.

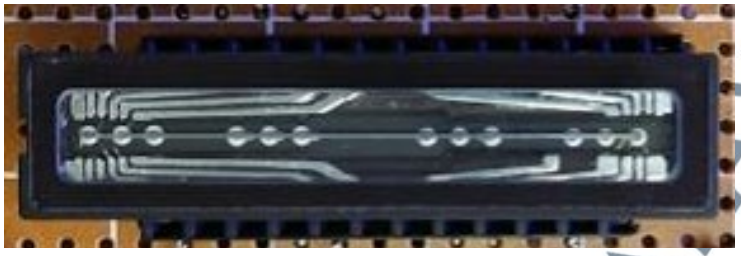

Figure 3.16: SONY™ ILX551A CCD Linear Sensor

Four CCDs provided 160 views, which was better in terms of accuracy than the 80 views from four CCDs used in previous studies (Jamaludin, Abdul Rahim, et al., 2018). Figure 3.17 shows the 2048 pixels of the 160 views of the CCD. Equation 3.20 indicated that the total number of pixels for every 40 views is ≈51. In the 40 views, total CCD voltage output values acquired from the 51 CCD pixels can be calculated to derive the mean value (Jamaludin, 2016). For total pixels of 40 views,

$$\frac{2048}{40} = 51.2 \tag{3.19}$$

The length per pixel of a SONY™ ILX551A CCD Linear Sensor is 0.014 mm (Sony Corporation, n.d.). Therefore, the length per pixel for 160 views was,

$$0.014 \text{ x } 51 = 0.714 \text{ mm} \tag{3.20}$$

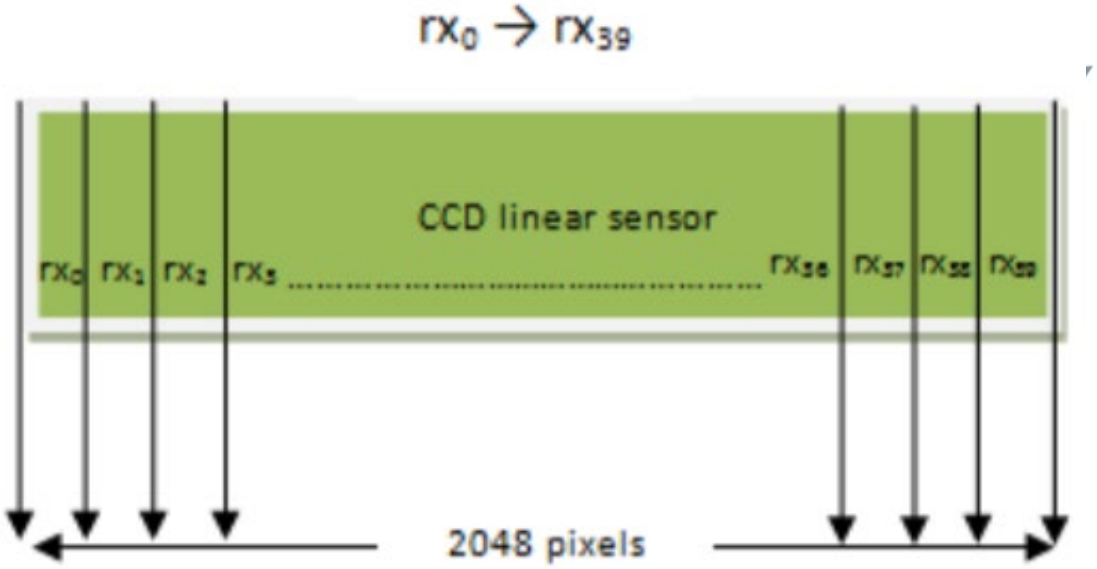

Source: Juliza & Rahim (2016)

Figure 3.17: The 2048 Pixels of the 160 Views of the CCD

As explained in 3.5.2.1 and 3.5.2.2, four projections represent the number of views by the CCD. And for each projection, there will be 40 views which summarize the 4 CCD will contribute 160 views which have better accuracy compared to only 20 views per CCD (Jamaludin, Abdul Rahim, et al., 2018). The graphical coding block diagram for this view's visualization is shown in Figure 3.18, Figure 3.19 and Figure 3.20. Meanwhile, Figure 3.21 and Figure 3.22 shows the single view of the LBP algorithm and the additional graphical code for the 3D image output, respectively.

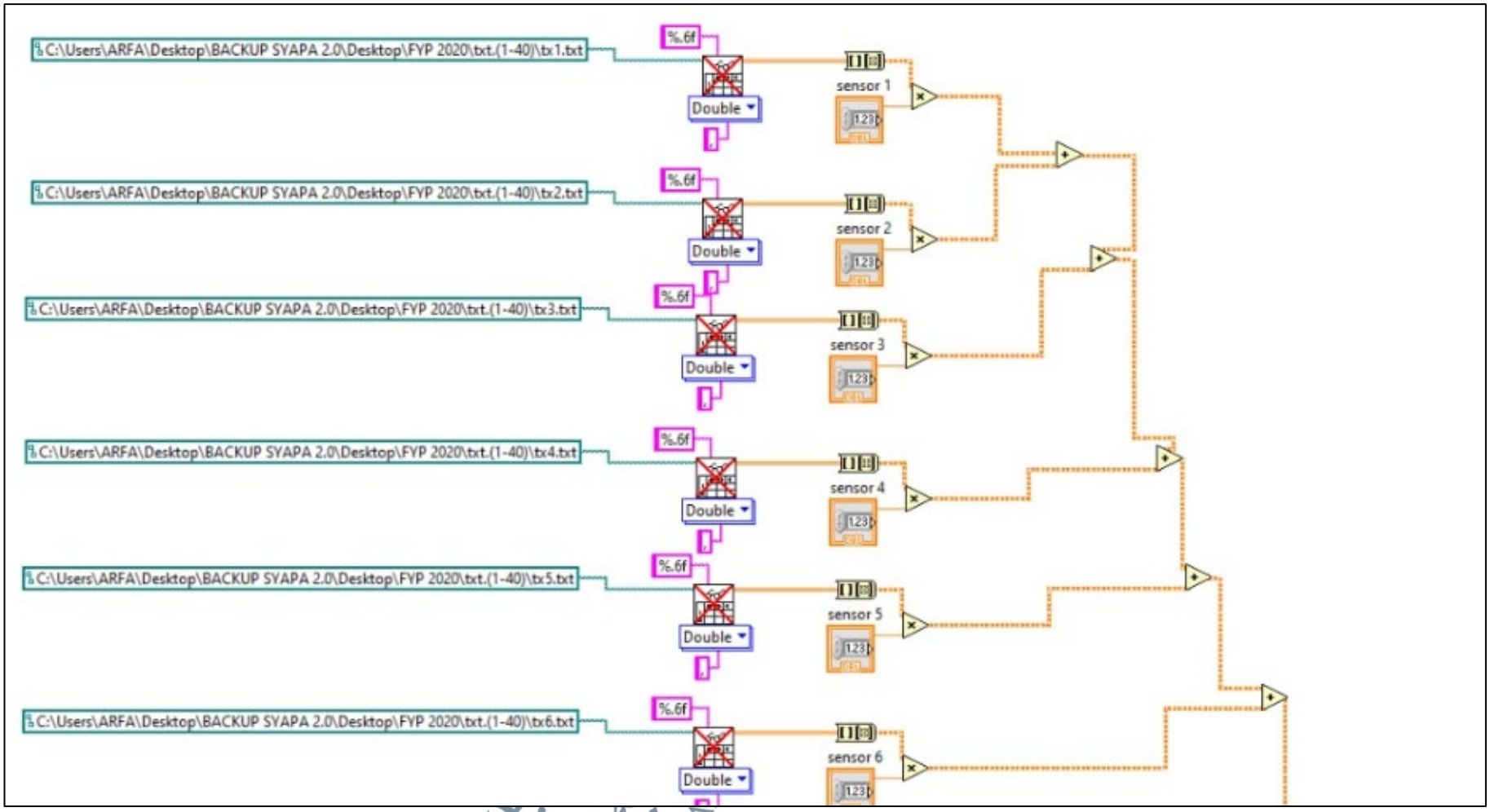

Figure 3.18: LabVIEW Graphical Coding for View 1 To 6 In The 1st Projection

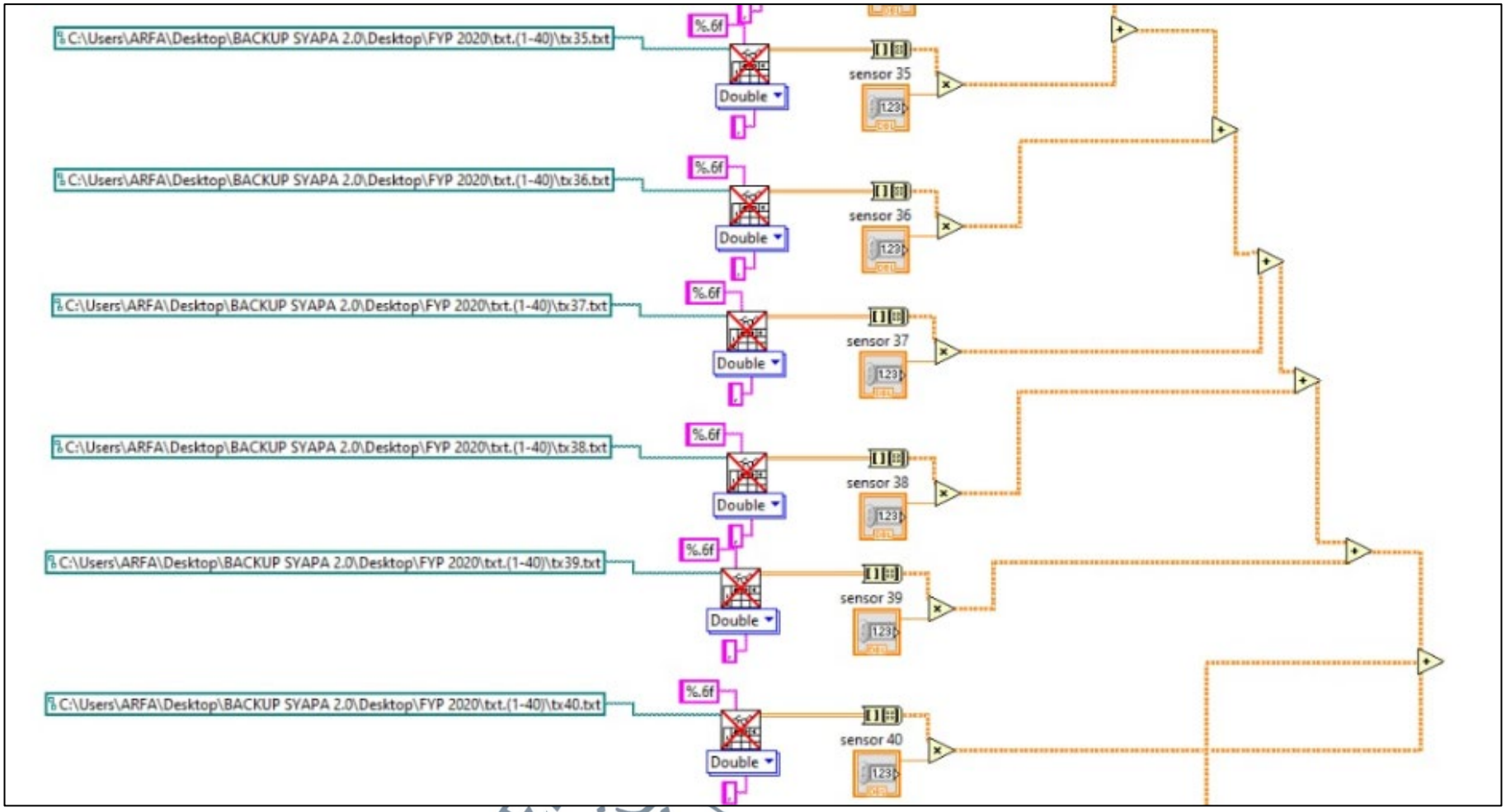

Figure 3.19: LabVIEW Graphical Coding for View 35 To 40 In The 1st Projection

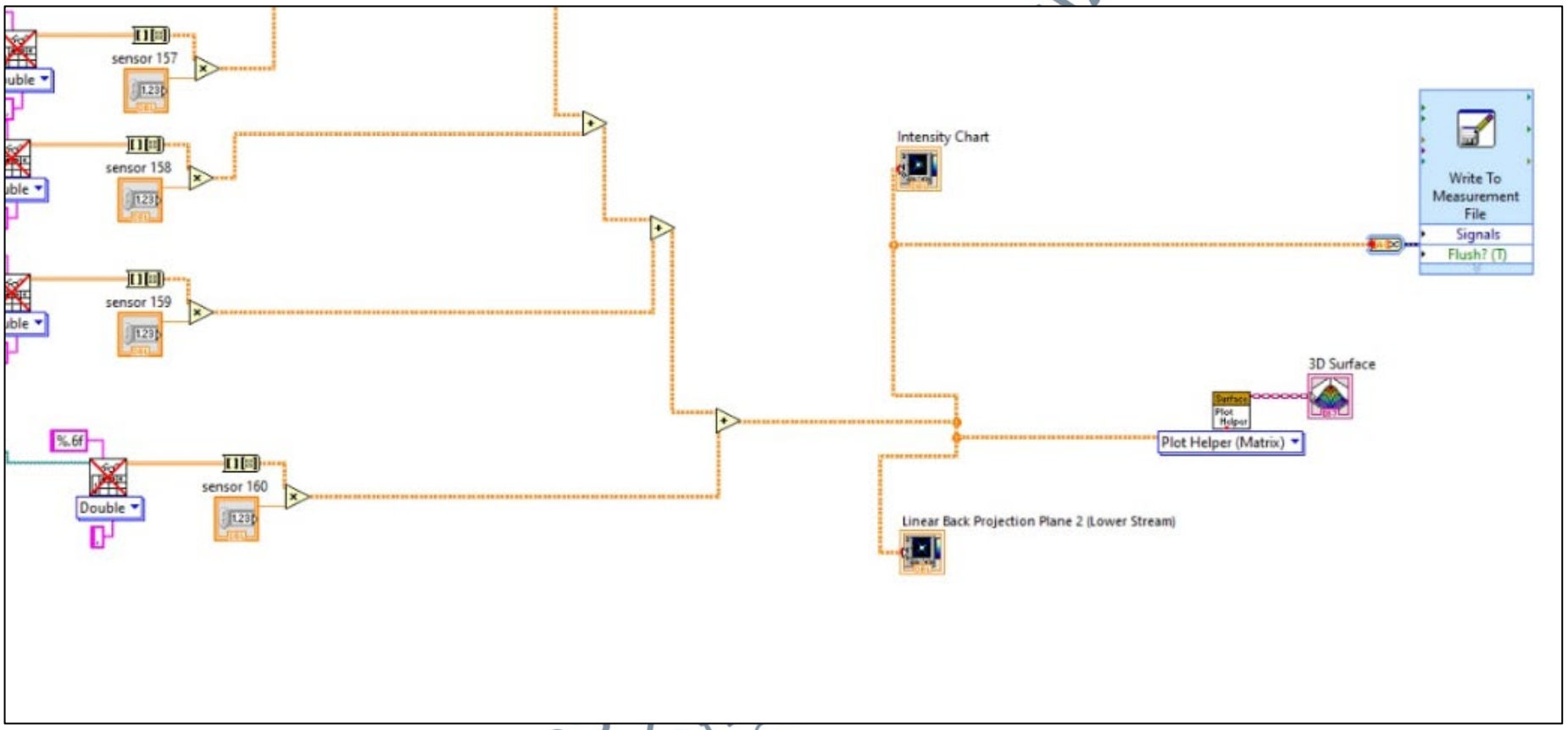

Figure 3.20: LabVIEW Graphical Coding for Views 157 To 160 In The 4th Projection

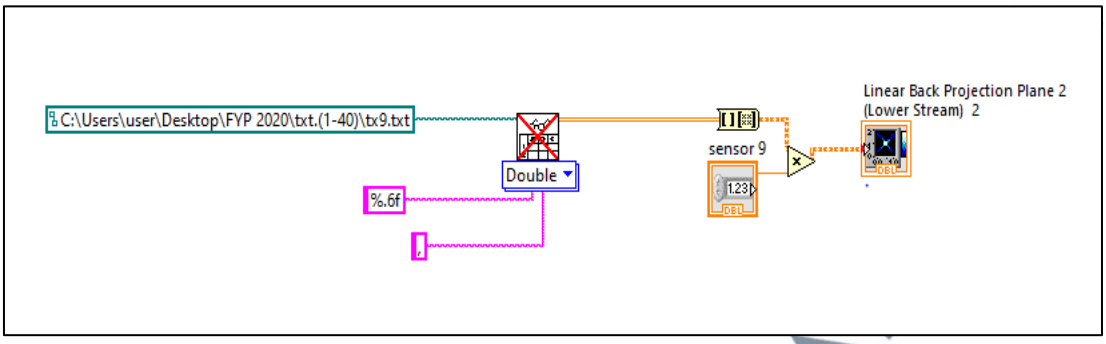

Figure 3.21: Single View of The Linear Back-Projection (LBP) Algorithm

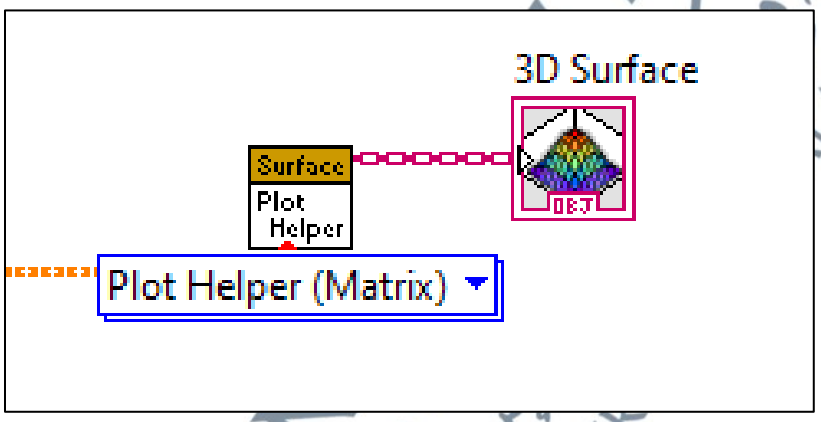

Figure 3.22: Graphical Code for the 3D Image Output

For each single projection view, the block diagram of function involved is the sensor, the function that could read from the spreadsheet file, the array to matrix function, the node of multiplication that multiplies the array to matrix function with the sensor, and, lastly to the 3D surface to enable the three-dimensional image reconstruction. Therefore, to gain the 160 views, 160 sensors were combined with different sensor values. The different sensor values will form pixels of various values that will evaluate the optical properties of ruby stone. The number of sensors used for 19.18 mm of ruby stone z was tabulated in Table 3.3 section 3.5.2.4.

3.5.2.3 Image Reconstruction Algorithm

In this study, the image was developed using the Linear Back Projection (LBP) algorithm that could be applied for the reconstruction analysis of 160 image views. This technique was repeated 160 times to acquire a clear picture. An increase in the number of pixels increases the number of sensors for the algorithm. The LBP algorithm has been used in this study as it is effective and convenient for processing the output image (Jamaludin, 2013a). Compared to other methods, the LBP method is one image reconstruction algorithm with fast and real-time imaging speeds (B. Sun et al., 2015). In reconstructing the image using LBP, each sensitivity matrix is multiplied with its corresponding sensor reading, which is convenient to use in image processing (Wahab et al., 2017). The equation that was used; Equation 3.21; is shown below:

$$V_{LBP\ (160views)}(x, v) = \sum_{tx=0}^{159} \sum_{rx=0}^{159} S_{tx,rx} M_{tx,rx} \tag{3.21}$$

Where $S_{tx,rx}$ is to the voltage value of the CCD output and V_{CCD} and $M_{tx,rx}$ are the sensitivity map (Jamaludin, 2016).

3.5.2.4 Simulation Model

The length of a single CCD, i.e., 28 mm, was considered to determine the number of sensors that should be used in this study. By dividing 28 mm over 40 views (sensors in LabVIEW), a value of 0.7 mm was obtained. Figure 3.3 depicts the diameter of ruby stone *z*, 19.18 mm, determined using a vernier caliper. The equation below shows the number of sensors to be used for the diameter of interest; 19.18 mm.

$$\frac{Size\ of\ diameter\ of\ interest}{0.7mm} \tag{3.22}$$

$$\frac{19.18mm}{0.7mm} = 27.4{\sim}27 \tag{3.23}$$

$$Number\ of\ sensors\ \ x\ 4\ views \tag{3.24}$$

As such, the total number of sensors used for a ruby stone measuring 19.18 mm in diameter was *27 x 4 = 108*. By rounding off to the nearest decimal number, it was determined that 27 sensors would be used for each of the CCDs in the flow pipe projection. Therefore, 108 sensors were used in the simulation model for a complete CCD measurement. Table 3.3 provides the division of the 108 sensors for a complete CCD measurement (four CCDs) based on the position of the CCDs and the laser, as seen in Figure 3.14. The simulation model provided the theoretical value used in this study. This model was crucial in analyzing the pixel value of the 3D ruby image based on the theoretical and experimental values to validate the ability of CCD tomography and LabVIEW programming software to produce a optical properties valuation of ruby stones based on statistical and relative error analysis.

Table 3.3: Number of Sensors Used for One Complete CCD Measurement

CCD	Number of Sensors
1	45, 46, 47, 48, 49, 50, 51, 52, 53, 54, 55, 56, 57, 58, 59, 60, 61, 62, 63, 64, 65, 66, 67, 68, 69, 70, 71, 72, 73, 74, 75
2	85, 86, 87, 88, 89, 90, 91, 92, 93, 94, 95, 96, 97, 98, 99, 100, 101, 102, 103, 104, 105, 106, 107, 108, 109, 110, 111, 112, 113, 114, 115
3	125, 126, 127, 128, 129, 130, 131, 132, 133, 134, 135, 136, 137, 138, 139, 140, 141, 142, 143, 144, 145, 146, 147, 148, 149, 150, 151, 152, 153, 154, 155
4	6, 7, 8, 9, 10, 11, 12, 13, 14, 15, 16, 17, 18, 19, 20, 21, 22, 23, 24, 25, 26, 27, 28, 29, 30, 31, 32, 33, 34, 35, 36

3.5.2.5 Monitoring the Model System for the Optical Properties of Ruby Stones in LABVIEW

Figure 3.23 illustrates the monitoring model system used to quantitatively grade ruby stone consisting of 160 partial views (sensor) from four CCDs and a 3D image reconstruction. The sensor turns ON based on the position and location of the ruby stone. By comparison, the value of the sensor indicates the voltage output of the CCD based on the final light intensity ratio of the CCD from the laser and ruby stone. The 3D image consisted of the z-axis, which represents the pixel value. The pixel value of the reconstructed image was then analyzed to measure the varying clarities of ruby stones to produce the quantitative grades of the ruby stones.

As described in Chapter 2, the CCD tomography techniques used three optical sensor modeling processes, which can be further used for sensitivity map applications. These include the optical path length technique, optical attenuation technique, and optical path width technique. This present study used the optical path and the optical attenuation methods to investigate the clarity and transparency of ruby stones (S. Ibrahim et al., 1999). The LBP algorithm refers to the sum of sensitivity matrixes used for every sensor that is then multiplied by a sensor voltage. Figure 3.23 shows that the z-axis, which represents the pixels gained, was equal to 221.74 when the value of the sensor was 1.994V. This 1.994V was also obtained during the previous mathematical expression when the final light intensity ratio was 0.8478 for a ruby stone RI of 1.762. The pixel values gained from the different ruby stones were used to validate the optical properties of various ruby stones.

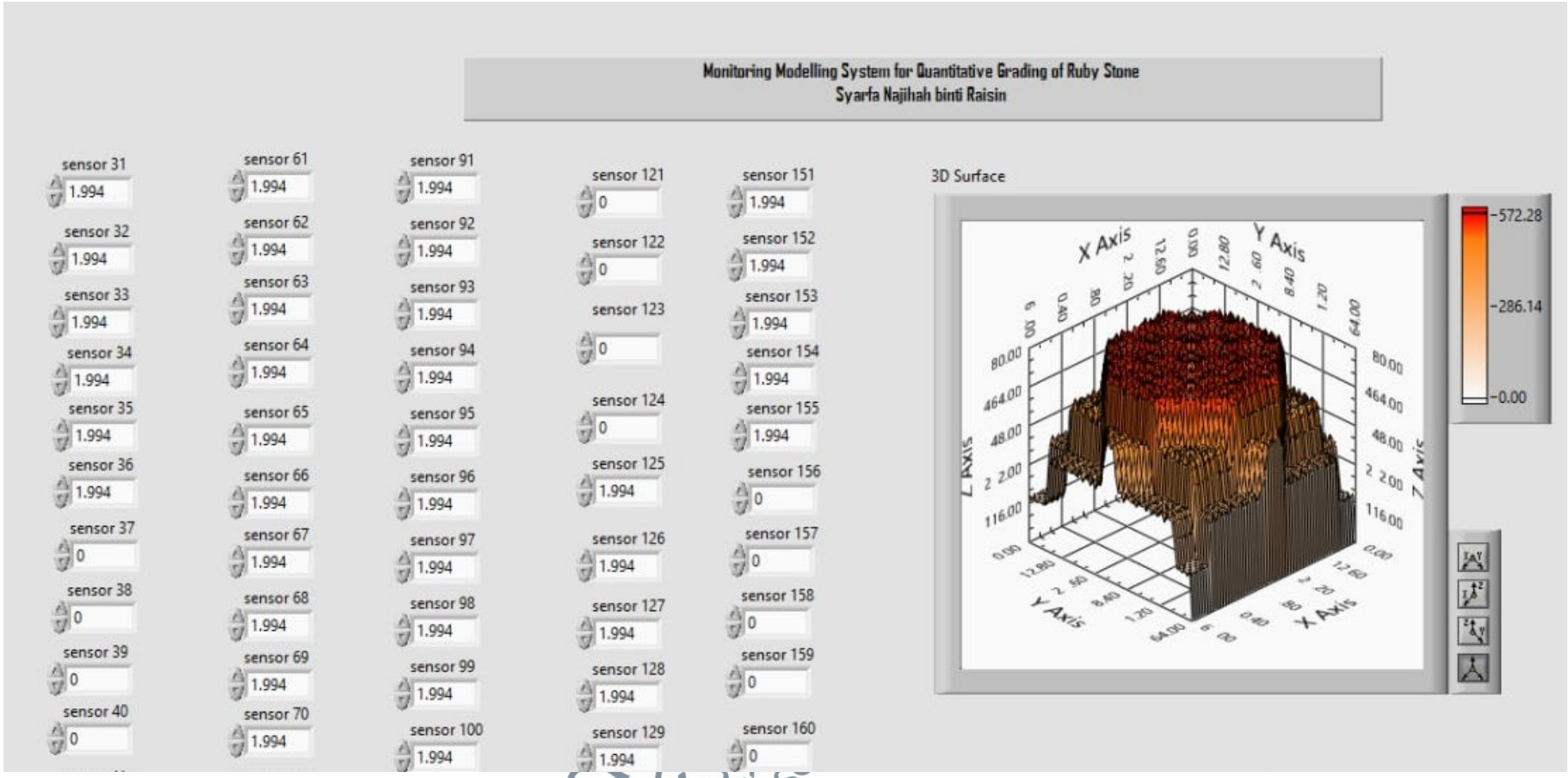

Figure 3.23: Image Reconstruction Modeling in LabVIEW